Classification and Prediction of Clinical Improvement in Deep Brain Stimulation From Intraoperative Microelectrode Recordings

Kyriaki Kostoglou, Konstantinos P. Michmizos, Pantelis Stathis, Damianos Sakas, Konstantina S. Nikita, and Georgios D. Mitsis*

***Abstract*—We present a random forest (RF) classification and regression technique to predict, intraoperatively, the unified Parkinson's disease rating scale (UPDRS) improvement after deep brain stimulation (DBS). We hypothesized that a data-informed combination of features extracted from intraoperative microelectrode recordings (MERs) can predict the motor improvement of Parkinson's disease patients undergoing DBS surgery. We modified the employed RFs to account for unbalanced datasets and multiple observations per patient, and showed, for the first time, that only five neurophysiologically interpretable MER signal features are sufficient for predicting UPDRS improvement. This finding suggests that subthalamic nucleus (STN) electrophysiological signal characteristics are strongly correlated to the extent of motor behavior improvement observed in STN-DBS.**

***Index Terms*—Deep brain stimulation (DBS), microelectrode recordings (MERs), Parkinson's Disease, random forests (RFs), subthalamic nucleus (STN), unified Parkinson's disease rating scale (UPDRS).**

I. Introduction

PARKINSON'S disease (PD) is a progressive neurodegenerative disorder that typically results in resting tremor, bradykinesia, rigidity, and postural instability [1]. One of the most effective treatments for PD is deep brain stimulation (DBS) of the subthalamic nucleus (STN) [2]–[4]. Although the clinical benefits of STN-DBS have been established since the '90 s [5], the mechanisms of how the DBS ameliorates the motor symptoms of PD have not been fully elucidated [6]. The procedure involves the surgical implantation of stimulation electrodes into the STN and provides a unique opportunity to record *in vivo* the related neuronal activity, through microelectrode recordings (MERs) of high spatial and temporal resolution. However, the optimal placement of the stimulation electrode continues to be a challenge, possibly due to the neuroanatomic variability within the STN sensorimotor area [7]. MERs have been used before to enhance our understanding of how STN neurons function [8]–[10] and identify possible mechanisms for DBS in PD [11]. MER-based algorithms have also been developed to identify the sensorimotor area within the STN by using both the high- [12]–[15] and low-frequency content [16] of the recorded signals. The high frequencies of the MER signal include both the action potentials from neurons located closest to the electrode tip (typically at a distance of less than 100–300 μm) [17] as well as smaller subnoise level spikes from nearby neurons known as background unit activity (BUA) [18], [19]. The combination of these two signals is termed multiunit activity (MUA). The lower frequencies of the MER signal correspond to the local field potential (LFP), which reflects the aggregate activity of a population of neurons within a larger diameter from the electrode tip (around 0.5–3 mm) [20]. Up to now, most of the MER-based analyses of the STN have focused on the gross automatic detection of the STN borders [12]–[15]. In [16], we have identified the extent of the pathophysiological beta band peak of the LFP as a potential neuromarker for guiding DBS contact placement within the sensorimotor area of the STN. Other studies have correlated LFP or MUA features with DBS improvement [21]–[25]; however, to our knowledge, no studies have sought to quantify and predict the subject-specific improvement.

In this study, we have followed a machine-learning approach in order to personalize the evidence-based DBS implantation procedure and validated it using 20 DBS patients. Currently, the intraoperative STN localization is based on the neurologist's empirical assessment of the electrode location [26] and, therefore, does not guarantee optimal motor improvement, given the neurophysiological and anatomical variability of the STN. The main goal of our study was to reveal the significance of intraoperative neural signals and elucidate their predictive role in terms of the response to STN-DBS. We used an ensemble of decision trees, known as random forests (RFs) [27], [28], which we have modified accordingly, and systematically identified MER features that can predict the DBS response for each patient with regards to their corresponding clinical improvement, as as-

Manuscript received September 18, 2015; revised June 14, 2016; accepted July 8, 2016. Date of publication July 18, 2016; date of current version April 18, 2017. This work was supported in part by the Natural Sciences and Engineering Research Council of Canada under Grant RPGIN- 2014-05931. K. P. Michmizos was supported by the Charles and Johanna Busch Biomedical Grant Award. *Asterisk indicates corresponding author.*

K. Kostoglou is with the Department of Electrical and Computer Engineering, McGill University.

K. P. Michmizos is with the Department of Computer Science, Rutgers University.

P. Stathis and D. Sakas are with the Department of Neurosurgery, National and Kapodistrian University of Athens.

K. S. Nikita is with the School of Electrical and Computer Engineering, National Technical University of Athens.

*G. D. Mitsis is with the Department of Bioengineering, McGill University, Montreal, QC H3A 0C3, Canada (e-mail: georgios.mitsis@mcgill.ca).

Digital Object Identifier 10.1109/TBME.2016.2591827

sessed by the unified Parkinson's disease rating scale (UPDRS) [29]. By using a heuristic binary "good" versus "poor" UPDRS improvement categorization, we classified correctly 19/20 patients using four MER features. We also predicted the UPDRS improvement with a normalized mean squared error (NMSE) of 3.37% using five MER features. To our knowledge, this is the first study that uses a machine-learning approach to predict the UPDRS improvement with high accuracy, based on a low number of neurophysiologically interpretable signal features.

II. Extracellular Recordings

A. Data Acquisition

MERs were obtained from 20 PD patients (seven female; mean age: 60.9 $\pm$ 6.30 years, mean disease duration: 14.8 $\pm$ 4 years) who underwent DBS surgery at the Neurosurgery Clinic, Evangelismos General Hospital, Athens, Greece [16]. All patients met the selection criteria of the core assessment program for surgical interventional therapies-PD protocol [30] and gave their informed consent. During surgery, patients were "off" dopaminergic medications. The quadripolar electrodes were stereotactically implanted into both hemispheres (bilateral stimulation) [31]. Target coordinates were defined on the basis of computerized tomography and intraoperative image fusion with three-dimensional (3-D) magnetic resonance imaging (MRI) images. A typical entry point is usually just anterior to the coronal suture, 2–3.5 cm from the midline and the angle varies between 20° and 45° from the midline in a coronal plane [31]. MERs were performed in 0.5-mm steps, starting 5 mm above the MRI-defined target, using five parallel microelectrodes in a cross "Ben Gun" configuration. The goal of MERs was to identify the characteristic discharge pattern of STN as well as movement-related activity (MRA). The "best" trajectory was considered as the one with the longest STN recordings and detectable MRA [7], [32]. The surgical procedure for placing the stimulation macroelectrode in the track MERs has a 1-mm precision, both horizontally and vertically [33]. Intraoperative current stimulation (60-μs pulse width, 130-Hz frequency, 0.5- to 5.0-V amplitude) verified the short-term clinical improvement and identified possible side effects. UPDRS data included in this study were from follow-ups of up to two years.

B. Data Processing and Feature Selection

We used MERs corresponding to spontaneous STN activity. LFP and MUA signals were acquired by low-pass and high-pass filtering the MERs at cutoff frequencies of 200 and 500 Hz, respectively. Spike detection was performed via MUA amplitude thresholding. Spike-related features were assessed by common spike train metrics [14], [15]. To examine the behavior of local neuronal populations, the BUA was extracted from the MUA following the procedure presented in [18] and [19]. In the same studies, it was suggested that the coherence between the MUA/BUA signal envelopes and the LFP may reveal coherent activity of small or large neuronal populations, respectively. Therefore, we computed the low-frequency envelopes of the MUA (EMUA) and BUA (EBUA) signals by low-pass filtering ($<$100 Hz) their instantaneous amplitude. We extracted power band ratios (power of the signal in a specific band divided by its total power) and peak-to-average power ratios of the LFP, EMUA, and EBUA signals in the delta (D; 1–4Hz), theta (T; 4–10 Hz), beta (B; 10–45 Hz), gamma (G; 45–100 Hz), and high gamma (HG; 100–200 Hz) frequency bands. The theta band was further split into low theta (4–7 Hz) and high theta/alpha (7–10 Hz). Overall, we observed that the latter was slightly more informative.

To identify temporal and spatial coordination of neural activity between brain structures, we estimated phase–amplitude (PAFC) and phase–phase (PPFC) cross frequency coupling between a lower (LF) and higher (HF) frequency subband of the LFP signal, whereby these subbands are defined as before (D, T, B, G, and HG) [34]. After normalizing and bandpass filtering the LFP signal within these subbands, we applied the Hilbert transform [35] to the resulting band-limited signals in order to obtain their instantaneous phase and amplitude. The HF amplitude was binned and averaged as a function of the LF phase, and the maximum difference in average amplitude was defined as the PAFC index. The same procedure was followed for computing the PPFC, where the HF amplitude was replaced with phase. We examined whether there was any LFP-locked spiking activity by computing the preferred phase of the recorded spike trains in terms of the corresponding LFP trace in the D, T, B, G, and HG frequency bands [36]. Specifically, we constructed a histogram of the spike times relative to the instantaneous phase of the band-limited LFP signal, normalized by the total number of spikes. The maximum value obtained from the normalized histogram was used as a phase-locking index (maxPL).

We also included the distance between the maximum aggregate beta LFP peak, weighted across parallel microelectrodes, and the stimulation contact [16]. Demographic and clinical history features like age, disease duration, gender, preponderance (more affected side), Hoehn and Yahr PD scale for disease progression, preoperative total daily dose of antiparkinsonian medication in levodopa equivalents (LED), as well as the 3-D coordinates of the stimulation contact were also included. The x (lateral–medial) and y (posterior–anterior) axis coordinates were defined based on the cross formulation of the five "Ben–Gun" microelectrodes. The z-axis (ventral–dorsal) was defined based on the electrode descent trajectory, whereby zero corresponds to the preoperatively identified STN target, while negative and positive values correspond to locations toward the cortex and deeper than the target, respectively. We assigned two average feature vectors obtained from all MERs to each patient, obtained from the left and right STN, respectively. This was done because in PD, the neurodegenerative process typically affects the dopaminergic innervation of the two striata in an asymmetric manner, resulting in a lateralized onset of motor symptoms with persisting asymmetry (preponderance) as the disease progresses [37]. Overall, for each STN MER, we extracted 89 features. A list of indicative features and their descriptions is given in Table I.

TABLE I
FEATURE NAMES AND DESCRIPTIONS

Name	Description	Name	Description
PowerX_{W}	Power band ratio of signal X in frequency band W	BR	Bursting rate
PKX_{W}	Peak to average power ratio of signal X in frequency band W	PB	Percentage of bursts
$\text{FmaxPKX}_{\text{W}}$	Frequency corresponding to maximum peak to average power ratio of signal X in frequency band W	FR	Firing rate
CVX_{W}	Coefficient of variation of signal X in frequency band W	stim_{E}	Coordinates of the stimulation contact on axis E, where E corresponds to x (lateral–medial),y (posterior–anterior), or z (ventral–dorsal)
PAFC_{WZ}	LFP phase–amplitude cross frequency coupling index between the phase in band W and amplitude in band Z	stimd	Euclidean distance of stimulation contact from the STN center
PPFC_{WZ}	LFP phase–phase cross frequency coupling index between the phase in band W and amplitude in band Z	dist	Euclidean distance of the MER from the stimulation contact
ZeroCrossX	Percentage of zero crossings in signal X	$\text{distpeak}_{\text{B}}$	Distance between the maximum aggregate beta LFP peak and the stimulation contact
SNRX	$20\log_{10}\left(\frac{\sigma_{\boldsymbol{X}}}{\sigma_{\boldsymbol{n}}}\right)$, $\sigma_{\boldsymbol{X}} = \text{std}(\boldsymbol{X})$, $\sigma_{\boldsymbol{n}} = \frac{\text{median}(\lvert\boldsymbol{X}\rvert)}{0.6745}$	hemi	Hemisphere (Left or Right)
maxCohXY	Maximum coherence between signals X and Y	prep	Preponderance (L/R: most affected body side is the right/left, controlled by the left/right hemisphere)
$\text{maxCohXY}_{\text{W}}$	Maximum coherence between signals X and Y in frequency band W	HY	Hoehn and Yahr PD scale
max_PL_{W}	Maximum phase locking index in band W for the LFP signal	levpre	Preoperative LED
MISI	Mean interspike interval	age	Age
SISI	Interspike interval standard deviation	years	Disease duration
CVISI	Interspike interval coefficient of variation	gender	Gender (female/male coded as 1/2)
PS	Percentage of spikes in the spike signal		

The signals X and Y correspond to LFP, EMUA, or EBUA. The frequency bands W and Z are defined as follows: delta (D; 1–4 Hz), theta (T; 4–10 Hz), beta (B; 10–45 Hz), gamma (G; 45–100 Hz), and high gamma (HG; 100–200 Hz). For example, $\text{maxCohXY}_{\text{W}}$ refers to the maximum coherence between LFP and EMUA, LFP and EBUA, or EMUA and EBUA in one of the aforementioned frequency bands.

III. METHODS

A. Random Forests

Decision trees [38] are a nonparametric-supervised learning method that use learned decision rules to predict the value of a target variable. They are computationally efficient and relatively easy to interpret and they can handle mixed variables (continuous and discrete). However, decision-tree learners may not yield good generalization performance.

The most efficient way to mitigate overfitting is by training multiple uncorrelated trees in an ensemble learner called RF, which can be used both for classification and regression [27], [28]. RFs can handle highly nonlinear interactions and they can cope with a small number of observations and a large number of predictors. During the training phase, each tree in the RF is trained using a different subset of the data (bootstrap aggregation) and features (random subspace method) randomly sampled with replacement. The data that are left out during the construction of each tree [out-of-bag (OOB) set] are used for validation purposes (see Fig. 1). As the forest building progresses, it generates an internal unbiased estimate of the generalization error (OOB error) which is then used to identify the most important variables. The final OOB prediction for a given observation is the average score achieved over all trees (regression) or the majority vote within the forest (classification), excluding trees that included this observation during their training phase. In this study, we used RFs both for classification and regression. In the former case, we extracted features that heuristically classified "good" and "poor" STN-DBS responders, defined as patients that exhibited an "off"-state UPDRS improvement above or below 38%, respectively [16], [39], [40]. In the latter case, we extracted features that predict the UPDRS improvement value.

B. Model Training and Validation

RFs were trained using subject-wise bootstrapping [41], taking separately into account the left and right hemisphere STN feature vectors of each subject [see Fig. 2(a)]. Each RF consisted of 300 trees. For classification, each tree was created by choosing randomly with replacement 7/9 "good" responders and 7/11 "poor" responders. Therefore, the training pool consisted of 14 feature vectors (seven patients $\times$ two hemispheres) labeled as 1 ("good"), and 14 feature vectors labeled as 0 ("poor"). The remaining 12 feature vectors (2 "good" responders and 4 "poor" responders) were used as the OOB set (see Fig. 1). A patient was classified as "good" responder if the average predicted "good" response probability obtained for the left and right STN feature vectors was equal or higher than 0.5. The predicted UPDRS improvement (%) was computed as the average prediction obtained from the left and right STN.

C. Model Performance

In the case of classification, we used the Matthews Correlation Coefficient (MCC) [42] for the OOB data as a performance metric, which is a class skew insensitive measure given by

$$\text{MCC} = \frac{\text{TP}\cdot\text{TN} - \text{FP}\cdot\text{FN}}{\sqrt{(\text{TP}+\text{FP})(\text{TP}+\text{FN})(\text{TN}+\text{FP})(\text{TN}+\text{FN})}} \quad (1)$$

where TN (TP) and FN (FP) are the numbers of correctly and incorrectly predicted "poor" ("good") response observations,

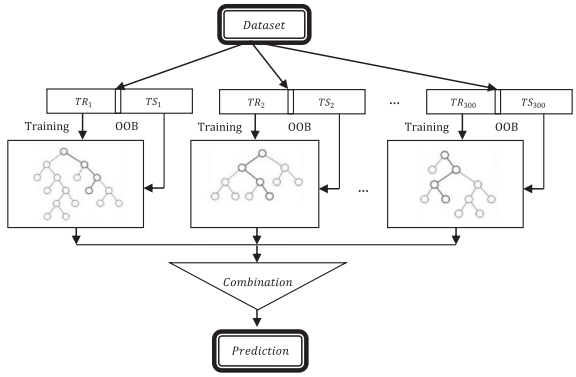

(a)

Random Forest Algorithm

1	Create 300 decision trees.
2	For each tree the training set consists of 7/9 "good" responders and 7/11 "poor" responders chosen randomly with replacement. The remaining 6 subjects are used as the OOB set.
3	Fit each tree to the training set.
4	Evaluate the performance of each tree on the respective OOB sets.
5	Identify the OOB sets to which a specific subject is included.
6	Extract the respective responses for the left STN and combine them using majority voting for classification or averaging for regression.
7	Repeat step 6 for right STN.
8	Obtain the final prediction by estimating the mean response from the left and right STN.
9	For classification: if the mean response is higher or equal to 0.5, label the patient as a "good" responder; otherwise, label as a "poor" responder. For regression: the predicted UPDRS improvement is the value obtained at step 8.
10	Repeat steps 5-9 for all subjects.
11	Estimate the MCC (classification) or the NMSE (regression) between clinically assessed and predicted responses of all subjects.
12	Assess FI using subject-wise permutation.
13	Remove the feature with the lowest FI.
14	Repeat steps 1-13 until no features are left (Backward elimination selection scheme).
15	Select the combination of features that yield the maximum MCC (classification) or minimum NMSE (regression).

(b)

Fig. 1. (a) RF with 300 trees. Each tree in the ensemble uses a different training (TR) and testing set (TS). (b) Algorithm and steps followed to acquire the prediction for each subject.

DATASET

Patient ID	Hemi	$PAFC_{DT}$	$PowerBUA_T$	…
81	R	0.713	0.161	…
	L	0.290	0.224	…
88	R	0.453	1.000	…
	L	0.375	0.187	…
91	R	0.344	0.000	…
	L	0.635	0.549	…
15	R	0.756	0.126	…
	L	0.604	0.316	…
101	R	0.557	0.087	…
	L	1.000	0.089	…
109	R	0.812	0.115	…
	L	0.492	0.158	…

(a)

TRAINING SET

Patient ID	Hemi	$PAFC_{DT}$	$PowerBUA_T$	…
81	R	0.713	0.161	…
	L	0.290	0.224	…
91	R	0.344	0.000	…
	L	0.635	0.549	…
101	R	0.557	0.087	…
	L	1.000	0.089	…
109	R	0.812	0.115	…
	L	0.492	0.158	…

OOB SET

Patient ID	Hemi	$PAFC_{DT}$	$PowerBUA_T$	…
88	R	0.453	1.000	…
	L	0.375	0.187	…
15	R	0.756	0.126	…
	L	0.604	0.316	…

OOB SET

Patient ID	Hemi	$PAFC_{DT}$	$PowerBUA_T$	…
88	R	0.453	1.000	…
	L	0.375	0.187	…
15	R	0.756	0.126	…
	L	0.604	0.316	…

OOB SET

Patient ID	Hemi	$PAFC_{DT}$	$PowerBUA_T$	…
88	R	0.756	1.000	…
	L	0.604	0.187	…
15	R	0.375	0.126	…
	L	0.453	0.316	…

(b)

Fig. 2. (a) Subject-wise bootstrapping. An example dataset with six patients and three representative features (Hemi, $PAFC_{DT}$, and $PowerBUA_T$) is presented. Red (blue) fonts indicate "poor" ("good") responders. Patients 81, 91, 101, and 109 were chosen randomly as a training set, whereas the remaining patients (88 and 15) were used as the OOB set. (b) An example of subject-wise permutation to estimate the FI of $PAFC_{DT}$ in the OOB set. In this case, the values of $PAFC_{DT}$ for Patient 88 replaced their counterparts for Patient 15 after swapping (the value corresponding to the right hemisphere was assigned to the left hemisphere and vice versa) and the values of $PAFC_{DT}$ for Patient 15 replaced their counterparts for Patient 88 without swapping.

respectively. An MCC value of 1 corresponds to a perfect prediction, while a value of –1 indicates a total disagreement between prediction and observation. Random classification yields values close to 0. In case of a tie in terms of the MCC value, we chose the classifier that yielded the minimum cross-entropy loss function (J) defined as

$$J = -\frac{1}{N}\left(\sum_{k=1}^{N} y_k \ln(p_k) + \sum_{k=1}^{N} (1-y_k)\ln(1-p_k)\right) \quad (2)$$

where N is the total number of subjects, y_k is the clinically assessed response of subject k, and p_k is the predicted response, i.e., the average predicted probability of "good" response from the left and right STN. When different classifiers exhibited the same predicted binary response, we selected the one that predicted, with higher (lower) probabilities, the "good" ("poor") responders. For example, if a subject (labeled as "good" responder) had been predicted as a "good" responder from two classifiers with probabilities 0.55 and 0.8, respectively, the second classifier would be selected. In the case of regression, model performance was assessed by using the Pearson correlation coefficient (ρ) and the NMSE between the predicted and the clinically assessed UPDRS improvement (%) output vector for the OOB data.

D. Feature Selection

RF feature importance (FI) is defined as the decrease in the predicted OOB MCC (classification) or increase in the predicted OOB NMSE (regression) if the values of this feature are randomly shuffled during the OOB phase of the RF algorithm. This measure was computed for every tree, averaged and divided by the standard deviation over the entire forest [27]. The idea behind this procedure is that if a feature is important, rearranging its values will have a negative impact on the prediction accuracy. On the other hand, if it is not important (noninformative), the predictive performance of the model will not be affected much. To account for subject-level dependencies between features, we additionally applied a subject-wise permutation scheme, whereby each variable was initially permuted randomly within subjects and subsequently permuted across

subjects. In other words, we randomly permuted the two (left and right STN) values of a given subject's feature and assigned them randomly to another subject [see Fig. 2(b)]. At each iteration, the feature with the lowest OOB FI was subsequently removed. The procedure was repeated until no features were left (backward elimination selection scheme) [43]. The combination of features that yielded the maximum MCC (classification) or minimum NMSE (regression) was selected.

IV. Results

A. STN-DBS Response Prediction

We treated the prediction of the STN-DBS response as a classification problem. We applied the backward elimination feature selection scheme described in Section III-D and found that four features achieved a maximum MCC value of 0.9045, with a confusion matrix C of the form

$$C = \begin{array}{cc} \boldsymbol{TN} & \boldsymbol{FP} \\ \left|\, 10 \right. & \left. 1 \,\right| \\ \left|\, 0 \right. & \left. 9 \,\right| \\ \boldsymbol{FN} & \boldsymbol{TP} \end{array} \begin{array}{c} . \\ \boldsymbol{N} \\ \boldsymbol{P} \\ . \end{array}$$

where $N = \mathrm{TN} + \mathrm{FP}$ is the total number of actual "poor" responders (11 in our case) and $P = \mathrm{FN} + \mathrm{TP}$ is the total number of actual "good" responders (9 in our case). In other words, only one "poor" responder was classified falsely in the "good" STN-DBS response group. The most significant features were found to be $\mathrm{PKLFP_{HG}}$, $\mathrm{PowerBUA_T}$, $\mathrm{maxPL_B}$, and $\mathrm{maxPL_{HG}}$ (see Table I) with FIs 0.1495, 0.9142, 0.3899, and 0.5982, respectively (backward elimination scheme). The effect of each feature on the model response is shown in Fig. 3(a). The plots were created by varying each feature at a time while keeping the rest fixed to their median values. Overall, there is a negative correlation between the values of the abovementioned features and the probability of "good" response, e.g., when $\mathrm{PKLFP_{HG}}$, $\mathrm{maxPL_B}$, and $\mathrm{maxPL_{HG}}$ attain their median values, an increase in the value of $\mathrm{PowerBUA_T}$ leads to a decrease of "good" response probability.

B. UPDRS Improvement After STN-DBS

In order to extract MER features that can quantitatively predict the improvement in the "off"-state UPDRS scale pre- and postoperatively, we used the backward elimination scheme as before. Five features achieved a maximum correlation coefficient of 0.9208, corresponding to an NMSE of 3.37%; $\mathrm{PowerBUA_T}$, $\mathrm{maxPL_B}$, $\mathrm{maxPL_{HG}}$, $\mathrm{PAFC_{DT}}$, and $\mathrm{PAFC_{TG}}$ (see Table I) with FIs 0.2067, 0.0651, 0.1507, 0.0834, and 0.1739, respectively. The clinically assessed and OOB predicted UPDRS improvement (%) for all patients is shown in Fig. 4. The effect of each feature on the model response can be seen in Fig. 3(b). $\mathrm{PowerBUA_T}$, $\mathrm{maxPL_B}$, and $\mathrm{maxPL_{HG}}$ were negatively correlated with the UPDRS improvement, while $\mathrm{PAFC_{DT}}$ and $\mathrm{PAFC_{TG}}$ were positively correlated with the latter.

We examined whether any of the extracted features were related to the underlying STN spatial characteristics by quantifying the correlations (Spearman's Rho) between the RF features and the 3-D coordinates of each MER for each patient and hemisphere. Five features, namely $\mathrm{PowerBUA_T}$, $\mathrm{maxPL_B}$, $\mathrm{maxPL_{HG}}$, $\mathrm{PAFC_{TG}}$, and $\mathrm{PKLFP_{HG}}$ were found to be significantly correlated to the MER coordinates within each subject and hemisphere. On the other hand, $\mathrm{PAFC_{DT}}$ was found to be unrelated with the MER locations in the majority of the patients.

V. Discussion

We predicted the response and UPDRS improvement of PD patients who underwent DBS, for the first time to our knowledge, with high accuracy by using a small subset of STN MER signal features. To achieve this, we used classification and regression RFs, modified to account for unbalanced datasets and multiple observations per patient. Due to the multiple observations (left and right STN), we used a subject-wise bootstrapping sampling method [41] to grow each individual tree within the forest. We extended this idea by applying a subject-level permutation-based FI measure where both intra- and intersubject variations were taken into account. Four MER signal features were found to be sufficient for predicting with high accuracy the DBS response, categorized here as "good" or "poor" response: $\mathrm{PKLFP_{HG}}$, $\mathrm{PowerBUA_T}$, $\mathrm{maxPL_B}$, and $\mathrm{maxPL_{HG}}$. The RF regression model identified five important STN features: $\mathrm{PowerBUA_T}$, $\mathrm{maxPL_B}$, $\mathrm{maxPL_{HG}}$, $\mathrm{PAFC_{DT}}$, and $\mathrm{PAFC_{TG}}$. Three of the five features were identical to the classification-related features ($\mathrm{PowerBUA_T}$, $\mathrm{maxPL_B}$, and $\mathrm{maxPL_{HG}}$) and were found to be negatively correlated with the clinically assessed improvement [see Fig. 3(b)].

The STN consists of three subregions: the sensorimotor (dorsolateral), associative (ventromedial), and limbic (medial) areas, as distinguished by their afferent and efferent projections [44]. These subregions exhibit different signal characteristics. Therefore, as the recording trajectories were not exactly the same for all subjects (see Section III), some of the recorded signal features may reflect (to some extent) neural activity that is specific to the aforementioned STN subregions probed by the microelectrode (recording bias). One of the limitations of this study is that we were not able to reconstruct a common 3-D coordinate system for all patients, since the exact entry point and trajectory angles for the microelectrodes were not available.

The most significant feature for both regression and classification was $\mathrm{PowerBUA_T}$, which was found to be anticorrelated to UPDRS improvement [see Fig. 3(b), Spearman $\rho = -0.440$; $p = 0.005$)]. Theta activity is tremor-related and consistent with the net driving of motor cortical areas at tremor frequencies through the GPi–thalamo–cortical pathway [45]. Theta oscillations in the basal ganglia have been previously linked with Parkinsonian and essential tremor [46], in contrast to alpha and beta STN oscillations which are common only among PD patients, suggesting a relation between theta activity and tremor irrespective of the underlying pathology. In particular, $\mathrm{PowerBUA_T}$ reflects the magnitude of the theta oscillatory activity in local neuronal populations, whereas $\mathrm{PowerLFP_T}$ reflects the activity of a larger population around the microelectrode. By examining the distribution of $\mathrm{PowerBUA_T}$ values along the z-axis, we observed an increase upon entering the STN, which is in accordance with

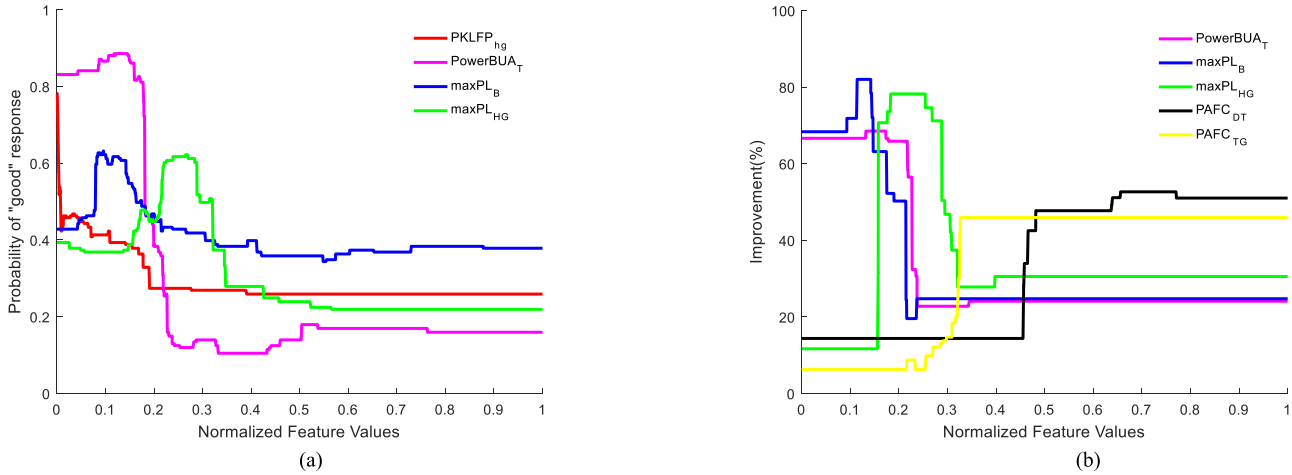

Fig. 3. Effect of each of the significant features on (a) the classification RF output (DBS response) and (b) the regression RF output (UPDRS improvement (%)). The plots were created by varying each feature at a time and keeping the rest fixed to their median values. The *x*-axis was normalized between 0 and 1 for all features.

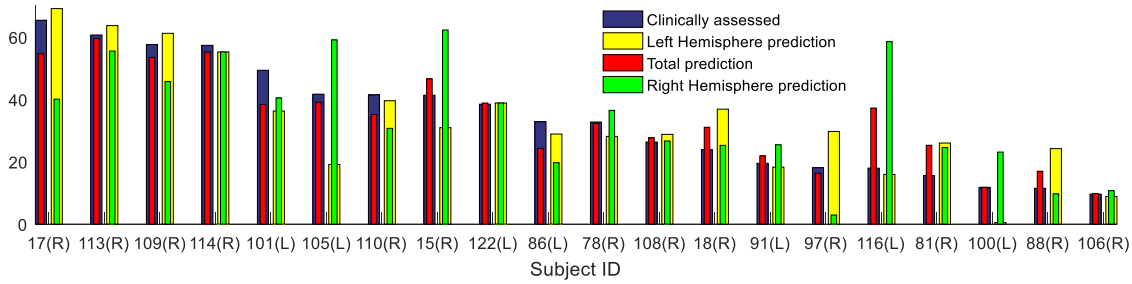

Fig. 4. Total predicted UPDRS improvement (%) and predicted improvement for left and right hemisphere (left and right panels: "good" and "bad" responders, respectively). The total prediction achieved for a subject was computed as the average prediction obtained from the two hemispheres. The letters inside the parentheses denote the clinical preponderance of the patient; L: left, R: right preponderance.

other studies which have suggested synchronized tremor-related activity in the dorsolateral sensorimotor region, where beta oscillatory and movement related neurons are typically located, using single-cell activity measurements [18], [26], [32], [47]–[52]. Collectively, these imply that PowerBUA_T is associated with local tremor units. Whether elevated PowerBUA_T is an inherent characteristic of the STN activity of "poor" responders or due to recording bias cannot be fully elucidated by our results. However, in a related study [19], the authors do not report significant differences between tremor frequency oscillating neurons and clinical subscores for tremor, rigidity, and bradykinesia, which suggest that these neurons do not exhibit different characteristics for different PD subtypes.

We speculate that basal ganglia circuitry dysfunction may lead to the association of the "poor" DBS response with high phase-locking in the beta band (maxPL_B). Note that the beta band is generally considered a feedback signal [53] and is prominent in the dorsal STN and globus pallidus of Parkinsonian patients withdrawn from their dopaminergic medication [54]. We observed that the high gamma LFP power ($\text{PowerLFP}_\text{HG}$) was anticorrelated with the beta ($\rho = -0.636$) and gamma ($\rho = -0.869$) activity, indicating that high gamma oscillations may reflect the action of different underlying LFP-generating mechanisms. Since maxPL_B and maxPL_HG are positively correlated to beta and high gamma LFP power, respectively, they may also reflect these mechanisms. PAFC_TG was also found to be positively correlated with LFP gamma power. In [52], increased low gamma LFP power was observed during periods of increased resting tremor especially in the dorsal STN, inducing an altered balance between beta and gamma rhythms. In [55], gamma band oscillations in the LFP were found to be synchronized to neuronal discharge in the upper (sensorimotor) STN and bordering *zona incerta* of PD patients, which has been recognized as one of the optimal sites for STN DBS.

PAFC_DT was found to be positively correlated to UPDRS improvement ($\rho = 0.408$, $p = 0.009$). Delta-driven PAFCs were not found to be dependent on location. On the other hand, theta-driven PAFCs were generally related with the location of the MERs, indicating an internal coupling inside the STN. Therefore, this may suggest that delta band information may originate from other brain structures. In [56], two distinct spatiotemporal couplings were found between the cerebral cortex and the STN in PD patients. The first one was manifested between 7 and 13 Hz and the second one was detected between 15 and 35 Hz. We observed that the effect of PAFC_DT was negative on the theta, beta, and gamma LFP power and positive on the

high gamma range. This effect was more pronounced in the beta band (especially between 22 and 35 Hz). Therefore, directly or indirectly, the delta phase had an attenuating role on the power of the LFP in the range of the modulated higher frequencies. Interestingly, "good" responders exhibited higher PAFC_{DT} than "poor" responders suggesting that perhaps patients with more pronounced cortical-STN interactions are more responsive to DBS.

In our recent work [16], we identified feature $\text{distpeak}_{\text{B}}$ as a marker for the location of the STN sensorimotor neurons which is associated with optimal DBS benefits. In this study, $\text{distpeak}_{\text{B}}$ was found in the top 8 and top 25 features in the classification and regression approach, respectively. Based on the aforementioned, beta power seems to be a "gross" metric able to discriminate between the heuristically derived "good" and "poor" DBS responses. The accurate prediction of the DBS response however requires, at least based on our results, the contribution of more localized features compared to $\text{distpeak}_{\text{B}}$. Clinical preponderance (the most affected side in the body controlled by the opposite hemisphere) and the hemisphere from which the MERs were recorded did not significantly affect the model prediction. This can be seen in Fig. 4, where the hemisphere corresponding to larger improvement in the "good" response group, was not necessarily the preponderant hemisphere. Overall, we found that taking into account information from both hemispheres for every feature yielded the best performance. This aligns with the common clinical practice of bilateral DBS since both sides are assumed to contribute to the response.

VI. Conclusion

The main goal of this study was to decipher the predictive role of intraoperative neural signals in STN DBS response and provide scientific insights by revealing the most informative intraoperative MER features and extracting STN MER "patterns" associated with UPDRS improvement. The results provide strong evidence that the proposed approach can employ a small number of the signal features inside the STN to predict, separately for each patient, the behavioral outcome of STN-DBS, justifying further investigation and, possibly, clinical applications.

References

[1] J. Jankovic, "Parkinson's disease: Clinical features and diagnosis," *J. Neurol. Neurosurg. Psychiatry*, vol. 79, no. 4, pp. 368–376, 2008.

[2] A. L. Benabid, "Deep brain stimulation for Parkinson's disease," *Curr. Opin. Neurobiol.*, vol. 13, no. 6, pp. 696–706, 2003.

[3] G. Deuschl *et al.*, "A randomized trial of deep-brain stimulation for Parkinson's disease," *New Engl. J. Med.*, vol. 355, pp. 896–908, 2006.

[4] F. Weaver *et al.*, "Bilateral deep brain stimulation vs best medical therapy for patients with advanced Parkinson disease," *J. Amer. Med. Assoc.*, vol. 301, no. 1, pp. 63–73, 2009.

[5] A. L. Benabid *et al.*, "Acute and long-term effects of subthalamic nucleus stimulation in Parkinson's disease," *Stereotact. Funct. Neurosurg.*, vol. 62, no. 1–4, pp. 76–84, 1994.

[6] S. Miocinovic *et al.*, "History, applications, and mechanisms of deep brain stimulation," *J. Amer. Med. Assoc. Neurol.*, vol. 70, no. 2, pp. 163–71, 2013.

[7] R. E. Gross *et al.*, "Electrophysiological mapping for the implantation of deep brain stimulators for Parkinson's disease and tremor," *Mov. Disord.*, vol. 21, pp. S259–S283, 2006.

[8] K. P. Michmizos *et al.*, "Prediction of the timing and the rhythm of the Parkinsonian subthalamic nucleus neural spikes using the local field potentials," *IEEE Trans. Inf. Technol. Biomed.*, vol. 16, no. 2, pp. 190–197, Jun. 2011.

[9] K. Kostoglou *et al.*, "Prediction of the Parkinsonian subthalamic nucleus spike activity from local field potentials using nonlinear dynamic models," in *proc. IEEE 12th Int. Bioinfo. Bioeng. (BIBE)*, pp. 298–302, 2012.

[10] K. P. Michmizos *et al.*, "Toward relating the subthalamic nucleus spiking activity to the local field potentials acquired intranuclearly," *Meas. Sci. Technol.*, vol. 22, no. 11, pp. 114021-1–114021-9, 2011.

[11] K. P. Michmizos and K. S. Nikita, "Addition of deep brain stimulation signal to a local field potential driven Izhikevich model masks the pathological firing pattern of an STN neuron," in *Proc. IEEE Annu. Int. Conf. Eng. Med. Biol. Soc.*, 2011, pp. 7290–7293.

[12] A. Moran *et al.*, "Real-time refinement of subthalamic nucleus targeting using Bayesian decision-making on the root mean square measure," *Mov. Disord.*, vol. 21, no. 9, pp. 1425–1431, 2006.

[13] P. Novak *et al.*, "Detection of the subthalamic nucleus in microelectrographic recordings in Parkinson disease using the high-frequency (>500 Hz) neuronal background. Technical note," *J. Neurosurg.*, vol. 106, no. 1, pp. 175–179, 2007.

[14] S. Wong *et al.*, "Functional localization and visualization of the subthalamic nucleus from microelectrode recordings acquired during DBS surgery with unsupervised machine learning," *J. Neural Eng.*, vol. 6, no. 2, p. 026006, 2009.

[15] H. Cagnan *et al.*, "Automatic subthalamic nucleus detection from microelectrode recordings based on noise level and neuronal activity," *J. Neural Eng.*, vol. 8, no. 4, p. 046006, 2011.

[16] K. P. Michmizos *et al.*, "Beta-band frequency peaks inside the subthalamic nucleus as a biomarker for motor improvement after deep brain stimulation in Parkinson's disease," *IEEE J. Biomed. Health Informat.*, vol. 19, no. 1, pp. 174–180, Jul. 2014.

[17] A. D. Legatt *et al.*, "Averaged multiple unit activity as an estimate of phasic changes in local neuronal activity: Effects of volume-conducted potentials," *J. Neurosci. Methods*, vol. 2, no. 2, pp. 203–217, Apr. 1980.

[18] A. Moran *et al.*, "Subthalamic nucleus functional organization revealed by Parkinsonian neuronal oscillations and synchrony," *Brain*, vol. 131, no. 12, pp. 3395–3409, 2008.

[19] A. Moran and I. Bar-Gad, "Revealing neuronal functional organization through the relation between multi-scale oscillatory extracellular signals," *J. Neurosci. Methods*, vol. 186, no. 1, pp. 116–129, 2010.

[20] U. Mitzdorf, "Properties of the evoked potential generators: Current source-density analysis of visually evoked potentials in the cat cortex," *Int. J. Neurosci.*, vol. 33, pp. 33–59, 1987.

[21] A. A. Kuhn *et al.*, "Pathological synchronisation in the subthalamic nucleus of patients with Parkinson's disease relates to both bradykinesia and rigidity," *Exp. Neurol.*, vol. 215, no. 2, pp. 380–387, 2009.

[22] S. Little *et al.*, "Beta band stability over time correlates with Parkinsonian rigidity and bradykinesia," *Exp. Neurol.*, vol. 236, no. 2, pp. 383–388, 2012.

[23] A. A. Kuhn *et al.*, "Reduction in subthalamic 8-35 Hz oscillatory activity correlates with clinical improvement in Parkinson's disease," *Eur. J. Neurosci.*, vol. 23, no. 7, pp. 1956–1960, 2006.

[24] C. C. Chen *et al.*, "Complexity of subthalamic 13-35 Hz oscillatory activity directly correlates with clinical impairment in patients with Parkinson's disease," *Exp. Neurol.*, vol. 224, no. 1, pp. 234–240, 2010.

[25] A. Zaidel *et al.*, "Subthalamic span of β oscillations predicts deep brain stimulation efficacy for patients with Parkinson's disease," *Brain*, vol. 133, no. 7, pp. 2007–2021, 2010.

[26] W. D. Hutchison *et al.*, "Neurophysiological Identification of the Subchaiarnic Xucleus in surgery for Parkinson's disease," *Ann. Neurol.*, vol. 44, pp. 622–628, 1998.

[27] L. Breiman, "Random forests," *Mach. Learn.*, vol. 45, no. 1, pp. 5–32, 2001.

[28] M. Fernández-Delgado *et al.*, "Do we need hundreds of classifiers to solve real world classification problems?," *J. Mach. Learn. Res.*, vol. 15, pp. 3133–3181, 2014.

[29] C. G. Goetz *et al.*, "Movement disorder society-sponsored revision of the unified Parkinson's disease rating scale (MDS-UPDRS): Scale presentation and clinimetric testing results," *Mov. Disord.*, vol. 23, no. 15, pp. 2129–2170, 2008.

[30] G. L. Defer, "Core assessment program for surgical intervention therapies in Parkinson's disease," *Mov. Disord.*, vol. 14, no. 4, pp. 572–584, 1999.

[31] D. E. Sakas and B. A Simpson (Eds.), *Operative Neuromodulation: Neural Networks Surgery*, vol. 2, Vienna, Austria: Springer, 2007, pp. 163–170.

[32] M. Rodriguez-Oroz *et al.*, "The subthalamic nucleus in Parkinson's disease: Somatotopic organization and physiological characteristics," *Brain*, vol. 124, pp. 1777–1790, 2001.
[33] J. Jankovic and E. Tolosa, *Parkinson's Disease and Movement Disorders*, Philadelphia, PA, USA: Lippincott Williams & Wilkins, 2007.
[34] R. T. Canolty and R. T. Knight, "The functional role of cross-frequency coupling," *Trends Cogn. Sci.*, vol. 14, no. 11, pp. 506–515, 2010.
[35] M. L. V. Quyen *et al.*, "Comparison of Hilbert transform and wavelet methods for the analysis of neuronal synchrony," *J. Neurosci. Methods*, vol. 111, pp. 83–98, 2001.
[36] A. G. Siapas *et al.*, "Prefrontal phase locking to hippocampal theta oscillations," *Neuron*, vol. 46, no. 1, pp. 141–151, 2005.
[37] K. L. Marek *et al.*, "[123I] beta-CIT/SPECT imaging demonstrates bilateral loss of dopamine transporters in hemi-Parkinson's disease," *Neurology*, vol. 46, pp. 231–237, 1996.
[38] J. R. Quinlan, "Induction of decision trees," *Mach. Learn.*, vol. 1, no. 1, pp. 81–106, 1986.
[39] A. Antonini *et al.*, "Brain flow changes before and after deep brain stimulation of the subthalamic nucleus in Parkinson's disease," *Neurol. Sci.*, vol. 24, no. 3, pp. 151–152, 2003.
[40] J. Herzog *et al.*, "Most effective stimulation site in subthalamic deep brain stimulation for Parkinson's disease," *Mov. Disord.*, vol. 19, no. 9, pp. 1050–1054, 2004.
[41] Y. V. Karpievitch *et al.*, "An introspective comparison of random forest-based classifiers for the analysis of cluster-correlated data by way of RF++," *PLoS One*, vol. 4, no. 9, p.e7087, 2009.
[42] B. W. Matthews, "Comparison of the predicted and observed secondary structure of T4 phage lysozyme," *Biochim. Biophys. Acta.—Protein Struct.*, vol. 405, no. 2, pp. 442–451, 1975.
[43] I. Guyon and A. Elisseeff, "An introduction to variable and feature selection," *J. Mach. Learn. Res.*, vol. 3, pp. 1157–1182, 2003.
[44] A. Parent and L. N. Hazrati, "Functional anatomy of the basal ganglia. II. The place of subthalamic nucleus and external pallidium in basal ganglia circuitry," *Brain Res. Rev.*, vol. 20, no. 1, pp. 128–154, 1995.
[45] P. Brown, "Oscillatory nature of human basal ganglia activity: relationship to the pathophysiology of Parkinson's disease," *Mov. Disord.*, vol. 18, no. 4, pp. 357–363, 2003.
[46] F. Steigerwald *et al.*, "Neuronal activity of the human subthalamic nucleus in the Parkinsonian and nonparkinsonian state," *J. Neurophysiol.*, vol. 100, no. 5, pp. 2515–2524, 2008.
[47] C. Reck *et al.*, "Characterisation of tremor-associated local field potentials in the subthalamic nucleus in Parkinson's disease," *Eur. J. Neurosci.*, vol. 29, no. 3, pp. 599–612, 2009.
[48] R. Levy *et al.*, "High-frequency synchronization of neuronal activity in the subthalamic nucleus of parkinsonian patients with limb tremor," *J. Neurosci.*, vol. 20, no. 20, pp. 7766–7775, 2000.
[49] M. C. Rodriguez *et al.*, "The subthalamic nucleus and tremor in Parkinson's disease," *Mov. Disord.*, vol. 13, pp. 111–118, 1998.
[50] F. Amtage *et al.*, "Tremor-correlated neuronal activity in the subthalamic nucleus of Parkinsonian patients," *Neurosci. Lett.*, vol. 442, no. 3, pp. 195–199, 2008.
[51] M. F. Contarino *et al.*, "Tremor-specific neuronal oscillation pattern in dorsal subthalamic nucleus of Parkinsonian patients," *Brain Stimul.*, vol. 5, no. 3, pp. 305–314, 2012.
[52] M. Weinberger *et al.*, "Increased gamma oscillatory activity in the subthalamic nucleus during tremor in Parkinson's disease patients," *J. Neurophysiol.*, vol. 101, no. 2, pp. 789–802, 2009.
[53] A. K. Engel and P. Fries, "Beta-band oscillations-signalling the status quo?" *Curr. Opin. Neurobiol.*, vol. 20, no. 2, pp. 156–165, 2010.
[54] P. Brown and D. Williams, "Basal ganglia local field potential activity: Character and functional significance in the human," *Clin. Neurophysiol.*, vol. 116, no. 11, pp. 2510–2519, 2005.
[55] T. Trottenberg *et al.*, "Subthalamic gamma activity in patients with Parkinson's disease," *Exp. Neurol.*, vol. 200, no. 1, pp. 56–65, 2006.
[56] V. Litvak *et al.*, "Resting oscillatory cortico-subthalamic connectivity in patients with Parkinson's disease," *Brain*, vol. 134, no. 2, pp. 359–374, 2011.

Authors', photographs and biographies not available at the time of publication.